Journal Pre-proof

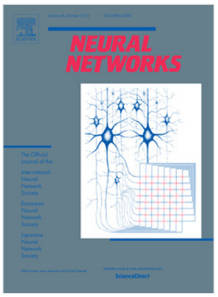

A bioinspired angular velocity decoding neural network model for visually guided flights

Huatian Wang, Qinbing Fu, Honxing Wang, Paul Baxter, Jigen Peng, Shigang Yue

PII: S0893-6080(20)30425-1
DOI: https://doi.org/10.1016/j.neunet.2020.12.008
Reference: NN 4669

To appear in: *Neural Networks*

Received date : 8 March 2020
Revised date : 3 December 2020
Accepted date : 7 December 2020

Please cite this article as: H. Wang, Q. Fu, H. Wang et al., A bioinspired angular velocity decoding neural network model for visually guided flights. *Neural Networks* (2020), doi: https://doi.org/10.1016/j.neunet.2020.12.008.

A Bioinspired Angular Velocity Decoding Neural Network Model for Visually Guided Flights

Huatian Wang[a,c], Qinbing Fu[c,a], Honxing Wang[c,a], Paul Baxter[a], Jigen Peng[b,c,*], Shigang Yue[c,a,*]

[a] *Computational Intelligence Laboratory (CIL), University of Lincoln, Lincoln, UK*
[b] *School of Mathematics and Information Science, Guangzhou University, Guangzhou, China*
[c] *Machine Life and Intelligence Research Center, Guangzhou University, Guangzhou, China*

Abstract

Efficient and robust motion perception systems are important pre-requisites for achieving visually guided flights in future micro air vehicles. As a source of inspiration, the visual neural networks of flying insects such as honeybee and Drosophila provide ideal examples on which to base artificial motion perception models. In this paper, we have used this approach to develop a novel method that solves the fundamental problem of estimating angular velocity for visually guided flights. Compared with previous models, our elementary motion detector (EMD) based model uses a separate texture estimation pathway to effectively decode angular velocity, and demonstrates considerable independence from the spatial frequency and contrast of the gratings. Using the Unity development platform the model is further tested for tunnel centering and terrain following paradigms in order to reproduce the visually guided flight behaviors of honeybees. In a series of controlled trials, the virtual bee utilizes the proposed angular velocity control schemes to accurately navigate through a patterned tunnel, maintaining a suitable distance from the undulating textured terrain. The results are consistent with both neuron spike recordings and behavioral path recordings of real honeybees, thereby demonstrating the model's potential for implementation in micro air vehicles which have only visual sensors.

*Corresponding authors
Email address: syue@lincoln.ac.uk (Shigang Yue), jgpeng@gzhu.edu.cn (Jigen Peng)

Keywords: Insect vision, motion perception, angular velocity, flight control, tunnel centering, terrain following.

1. Introduction

Executing delicate flight maneuvers using visual information is challenging for micro air vehicles (MAVs). Due to their small size and limited computing capabilities, it is difficult to install a global positioning system (GPS) or inertial navigation system (INS) onboard. Alternative solutions can be learned from the study of flying insects like honeybees, which possess limited neural resources but can deal with very complex visual flight tasks. The way insects visually detect motion has been a subject of study for many decades. However, the neural mechanisms involved in behaviors such as patterned tunnel centering [1, 2] and textural terrain following [3, 4, 5] are still not fully elucidated. According to the results of behavioral experiments on honeybees, the key to their extraordinary flight control is their ability to estimate and regulate angular velocity [6, 7, 8]. In these studies, honeybees fly along the central path of a narrow patterned tunnel with gratings of different spatial frequencies on both walls. The flight trajectory shifts towards a wall that is moving along the flight direction, whilst away from a wall that is moving in the opposite direction. This behavior indicates that honeybees adjust their positions by balancing the angular velocities estimated with both eyes[1]. Electro-physiological experiments have also revealed that the electrical activities of some descending neurons in the honeybee's ventral nerve cord increase as the angular velocity of the stimulus grating movement increases [9, 10], and the responses are largely insensitive to spatial frequency. Modelling of the honeybee's ability to estimate angular velocity is now commonly used in the design of flight control systems for MAVs that rely on visual inputs.

The angular velocity here is defined by the angular displacement $\Delta\phi$ of the image motion during a small time interval Δt, that is $\omega = \Delta\phi/\Delta t$. In tunnel centering and terrain following scenarios, denoting v_x as the forward flight speed and d as the distance to the surface, the angular velocity of image motion on the

retina can also be expressed as $\omega = v_x/d$. If the forward speed is maintained by a suitable constant forward thrust, then the distance to the surface will change automatically either by balancing the lateral angular velocities on both sides in tunnel centering [1], or by regulating the ventral angular velocity to a constant value in terrain following [5]. The question is, therefore, how do honeybees estimate the angular velocity and further regulate it?

To extract the angular velocity of the image motion on the retina, we have proposed an angular velocity decoding model (AVDM). The model consists of three parts: firstly a set of elementary motion detection circuits, secondly, a wide-field texture estimation pathway and thirdly, an angular velocity decoding layer. By combining both texture and temporal information from the input signals, the model estimates the angular velocity well when tested by moving sinusoidal gratings. Furthermore, together with the proposed control schemes, the model has reproduced visually guided flight behaviors including tunnel centering and terrain following activities of bees.

In summary, this work makes a threefold contribution:

- It is well known that the tunnel centering capability of honeybees is barely affected by the spatial frequency of the wall gratings[2]. The proposed model competently estimates the angular velocity of the retinal image motion and demonstrates improved spatial frequency independence when compared with previous angular velocity detecting models[11, 12], thereby explaining the flight behaviors of honeybees more efficiently.
- The spatial and temporal resolutions have been considered to obtain bio-plausible parameter settings in our simulations. Using the angular velocity balancing strategy, our model reproduces most of the tunnel centering and terrain following behaviors of honeybees.
- Our code and demonstration videos are publicly available [1]. These will

[1] Code for all modelling is available at `https://github.com/skyhouse123/AVDM_Unity`. Demonstration videos can be found at `https://youtu.be/gNvtaSqNjdI` and `https://youtu.be/l3SAnmOrgfk`.

help others to reproduce the simulations easily and perform further visual flight research based on current platform. In addition, the proposed model can be used in MAVs for visually guided flights using only visual sensors.

The work in this paper is a substantial extension of our previous conference work [13][14]. Advances reported in this paper are summarized as follows. First, a Lipetz transform [15] and an indicator of spatial dependence have been introduced to show that our model outperforms other models in testing spatial independence of the gratings. Second, in moving grating experiments, the robustness of the model in relation to various visual contrasts and noise levels have been examined. These are important criteria for model verification which previous research has not considered. Third, in tunnel centering simulations, a series of new experiments including an X-shape tunnel, a tunnel with gratings of different spatial frequencies, and wall movement at various speeds, have been designed to demonstrate the capability of the model to reproduce numerous flight behaviors of bees. Finally, in terrain following simulations, the model performance has been improved significantly. A series of controlled trials to check the influence of initial height, flight speed, and terrain pattern, have also been discussed to verify the feasibility of the proposed model across a range of scenarios.

The rest of this paper is organized as follows. First we present related work in Section 2. The formulation of the model is described in Section 3. The control schemes for tunnel centering and terrain following are described in Section 4. In Section 5, the results of synthetic grating experiments are exhibited to show the model's independence of both the spatial frequency and contrast of the grating. In addition, the model is tested behaviorally using a virtual bee for tunnel centering and terrain following in a series of controlled simulations. Finally, we discuss the research further and draw together our conclusions in Section 6.

2. Related Work

Due to the limited computation resources provided by the tiny insect brain, traditional computer vision methods, such as differential techniques, feature detection and matching, deep learning approaches are restricted here in explaining insects' visual motion detections [16, 17]. Biological models usually correlate the light intensities of neighboring photoreceptors using temporal filters rather than calculate the spatial or temporal gradient of images [18]. Hassenstein and Reichardt [19] proposed the first correlation motion detector, HR detector, which uses the temporal delay signal from a left arm to multiply a non-delayed signal from a right arm to detect motion. In a modified version, the HR-balanced detector has been proposed which, consists of two mirror-symmetrical subunits in conjunction with a balance parameter [20]. The HR-detector based angular velocity sensor [21] has been successfully used in enabling flight control tasks in visually guided aircraft by Franceschini and Ruffier [22] [23]. However, both the HR model and the HR-balanced model are tuned for a particular temporal frequency (number of gratings passed over the photoreceptor per second) rather than angular velocity [20]. Therefore, the output of their sensors show a large variance for flights tested against patterned ground [21].

Based on their numerical analysis, Zanker et al. [20] suggest that the ratio of outputs from two HR-balanced detectors can produce a response tuned for angular velocity. Following this idea, Cope et al. [12] proposed a model for estimating angular velocity using the ratio of two HR-balanced detectors with different temporal delays. However, the spatial independence of their model decreases as the velocity increases. Riabinina and Philippides[11] have also built a model using a channel fully dependent on temporal frequency as the denominator to obtain an angular velocity tuned response. However, the spatial independence weakens as the motion speed increases. Being inspired by the neural structure of Drosophila's visual system, Wang et al. [24] proposed a new motion detector with three inputs to produce a partially spatial independent response. Nevertheless, the model still does not show enough spatial

independence to explain the flight behaviors of honeybees.

The three models previously mentioned [11, 12, 24] each use the ratios of two channels to tune a response for angular velocity. This approach may cause a problem in the form of high outputs when the denominator is very small. It is also one of the reasons why their models do not perform well when the angular velocity of the moving grating is low or high. This limitation has inspired us to build a model that avoids using the ratio of two channels, but which combines the spatial and temporal information from the moving gratings, based on the assumption that there are mechanisms that combine both environmental texture and optic flow information in insect brains [25, 26].

Since insect compound eyes normally have thousands of ommatidia and a much higher temporal resolution than human eyes, it is possible to obtain textural information from wide-field neurons and temporal frequency information from spatially distributed HR-balanced detectors. We find that under a biologically high sampling rate, the temporal frequency of grating movement can be approximated by a nonlinear function when it is less than 50 Hz. Building on this idea, we propose an angular velocity decoding model, and implement it into tunnel centering[13] and terrain following[14] simulations to successfully reproduce behaviors of real bees. However, only preliminary ideas have been presented in previous work. A series of systematic experiments need to be performed to verify the effectiveness of the model.

3. Methods

3.1. Input Signal Simulation

To explain the flight behaviors of honeybees, the spatial and temporal resolutions of honeybees have been initially investigated to obtain bio-plausible parameter settings. The ommatidia of their bilateral compound eyes are arranged hexagonally, separated by the interommatidial angle $\Delta\varphi$ (approximately 2°, but they vary in different regions [27]) and each ommatidia corresponds to a visual column with an acceptance angle $\Delta\rho$ (approximately 2.5° [28]), as shown in Fig.

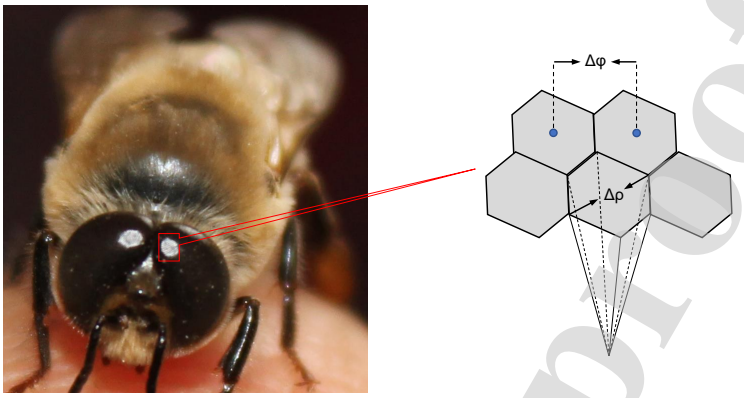

Figure 1: Illustration of the honeybee's compound eye structures. The ommatidia are arranged hexagonally with an angular separation $\Delta\varphi$ (interommatidial angle) and each has its own small receptive field $\Delta\rho$ (acceptance angle).

1. As for temporal resolution, the critical fusion frequency (beyond which honeybees show no response to the flickering light source in an electroretinogram test) is 165-300 Hz [29]. However, behavioral experiments indicate that honeybees can detect light fluctuations only when the stimuli are moving at temporal frequencies of less than 200 Hz [30]. Therefore, we set the sampling rate as 200 Hz, in accordance with the high temporal frequency image processing capability of the honeybee. Our proposed model is designed to deal with this high rate of data sampling. The performance in estimating angular velocity is improved by using such a high sampling rate.

The input signals are simulated using two-dimensional image sequences of sinusoidal gratings moving across the field of view. If λ and ω are the spatial period and the angular velocity of the grating movements respectively, then the temporal frequency and angular frequency can be computed as ω/λ and $2\pi\omega/\lambda$. Supposing the angular separation between pixels is φ (set to 2° in accordance with the honeybee's spatial resolution), the input images can be expressed as follows:

$$I(x, y, t) = (\sin(2\pi\omega/\lambda(t - \varphi(y - 1)/\omega)) + 1/C_t)/(1/C_t + 1) \quad (1)$$

where (x,y) denotes the location of the ommatidium, t indicates the time and $C_t \in (\xi, 1]$ is a parameter for tuning the contrast of the gratings. Regarding our moving grating setting, C_t happens to be the image contrast at time t under Michelson contrast definition:

$$\frac{I_{max}(t) - I_{min}(t)}{I_{max}(t) + I_{min}(t)} = \frac{\frac{2C_t}{1+C_t}}{2 - \frac{2C_t}{C_t+1}} = C_t \tag{2}$$

where the $I_{max}(t)$ and $I_{min}(t)$ $(I_{max}(t), I_{min}(t) \geq 0)$ indicate the highest and the lowest light intensities of the input signal at time t. For simplicity, we set the contrast of the grating as 1, except when considering the contrast invariance of the model.

3.2. Angular Velocity Decoding Model

The model contains three parts: the texture estimation pathway for extracting spatial information, the motion detection pathway for extracting temporal information extraction, and the decoding layer for estimating angular velocity. The structure of the proposed model is shown in Fig. 2. The spatial frequency and image contrast information are estimated by the texture estimation part, and the motion information is processed by motion detectors. The angular velocity is then decoded by combining both sets of information.

3.2.1. Texture estimation pathway

The simulated input signals received by the retina are first processed by the texture estimation pathway where the image contrast and the spatial frequency of the grating are estimated by the light intensities at different locations. This is based on a hypothesis that insects sense the complexity of textures. This is especially the case for honeybees, which can discriminate patterns by visual cues including edge orientation, size, and disruption [31]. Tunnel experiments also indicate that honeybees can distinguish the contrast on the wall at levels as low as 3%, and that flight speed in a tunnel is little affected by contrast, provided that the contrast is larger than 3% [32]. One possible neural mechanism involves estimating the contrast and eliminating its effect in the final response by the

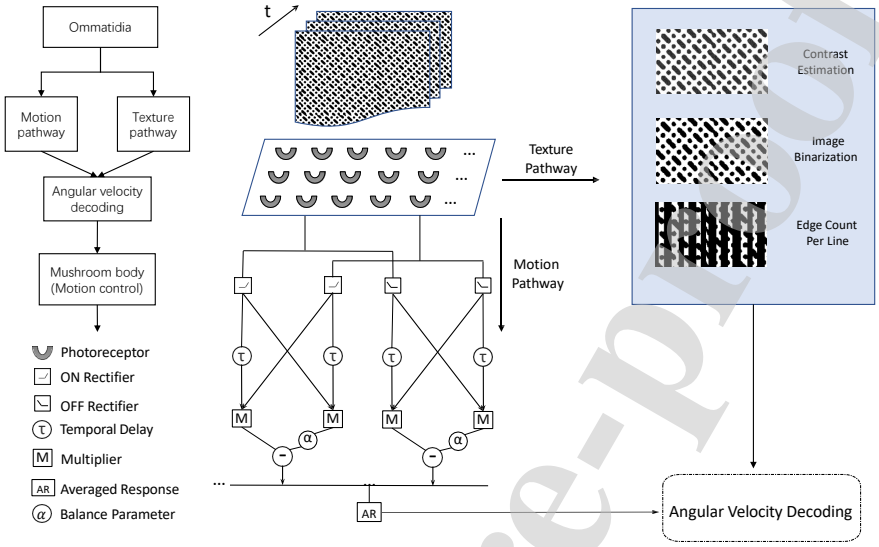

Figure 2: The structure of the proposed Angular Velocity Decoding Model. The visual information of grating movement is received by the ommatidia. The textural information and the motion information across the whole vision field are combined in the angular velocity decoding layer.

estimated value. Following this idea, the texture estimation pathway is proposed to establish the image contrast and spatial frequency using simple computations.

Following the setting that every ommatidium covers 2° (φ) view [27], with 60 vertical (M) by 66 horizontal (N) receptors per eye covering the view of 120° by 132°, we can estimate the image contrast $\widehat{C}$ and the spatial period $\widehat{\lambda}$ of the gratings according to the light intensities across the visual field. First the image contrast is estimated dynamically by the highest and lowest intensities, that is

$$\widehat{C}(t) = \frac{I_{max}(t) - I_{min}(t)}{I_{max}(t) + I_{min}(t)}. \tag{3}$$

The input image is then transferred into a binary image $I_B(t)$ with the intensity threshold $I_{thre}(t) = (I_{max}(t) - I_{min}(t))/2$. The spatial period is estimated by counting the number of boundary lines of the binary image within the whole visual field, which can be expressed as

$$\widehat{\lambda}(t) = \frac{2MN\varphi}{\iint |I_B(x, y+1, t) - I_B(x, y, t)| dxdy}. \quad (4)$$

This is a very computational efficient method to estimate the spatial frequency of sine-wave and square-wave gratings in our simulations. For more complex and detailed background, the method can also indicate the complexity of the textured background to some extent. A bank of linear spatial filters such as Gabor filters may help in this situation to extract texture information better.

3.2.2. Motion detection pathway

1) **Ommatidia:** We denote $I(x, y, t) \in R^3$ as the input image sequences, where x, y, t are spatial and temporal positions. The visual information is first processed in the retina where the light intensities are captured and smoothed by ommatidia which can be simulated using a Gaussian spatial filter [33]. The output is given by

$$P(x, y, t) = \iint I(x - u, y - v, t) G(u, v) du dv \quad (5)$$

where G(u,v) is a Gaussian kernel defined as

$$G(u, v) = \frac{1}{2\pi\sigma^2} \exp(-\frac{u^2 + v^2}{2\sigma^2}). \quad (6)$$

2) **Lamina layer:** To facilitate motion detection, the visual system of honeybees is more sensitive to changes in intensity than to absolute intensity. Therefore, in our model the input image frames are processed by the lamina layer where the light intensity changes are computed to obtain primary visual motion information [34]. Each photoreceptor computes the luminance change as follows:

$$L(x, y, t) = \int P(x, y, t - u) H_1(u) du + \int L(x, y, t - u) H_2(u) du \quad (7)$$

where $L(x, y, t)$ corresponds to the luminance change of pixel (x,y) at time t. $H_1(u)$ is a temporal filter defined as the subtraction of two impulse functions

$H_1(u) = \delta(u) - \delta(u - \tau)$, where the impulse function is

$$\delta(u) = \begin{cases} +\infty & u = 0, \\ 0 & u \neq 0. \end{cases}$$

$H_2(u)$ donates the temporal filter representing the persistence of the luminance change which is

$$H_2(u) = (1 + e^{\mu u})^{-1}. \tag{8}$$

3) **ON and OFF layer:** Inspired by the visual system in the fly[35], the luminance changes are separated into two pathways: the ON and the OFF pathways. Specifically, the ON pathway deals with light intensity increments; whilst the OFF pathway processes brightness decrements[36]. Denoting $f^+ = \max(0, f)$ and $f^- = \min(0, f)$, then we can express the outputs of the cells in ON and OFF pathways as $L^+(x, y, t)$ and $L^-(x, y, t)$ respectively. Having two parallel processing pathways ensures that honeybees navigate efficiently in a complex environment. We adopt these pathways in our model.

4) **Delay-and-correlation layer:** Denoting $D^+(x, y, t)$, $D^-(x, y, t)$ as the outputs of the ON and OFF detectors and τ as the temporal delay in HR-balanced detectors, we have the following expression according to the structure of motion detectors in Fig. 3, where each pairwise neighboring ON/OFF cells correlate with each other as:

$$D^+(x, y, t) = L^+(x, y, t - \tau) \cdot L^+(x, y + 1, t) - \alpha L^+(x, y, t) \cdot L^+(x, y + 1, t - \tau) \tag{9}$$

where α is chosen as 0.25 to form a partial balanced model[20]. $D^-(x, y, t)$ can be expressed similarly.

3.2.3. Angular velocity decoding layer

A honeybee's compound eyes contain thousands of ommatidia, each of which has its own angular orientation and acceptance angle [37]. In our model, there are many parallel detectors corresponding to all the visual columns. However, due to their various spatial positions, their responses differ slightly. We assume

that different detectors make diverse contributions towards the final response according to their spatial positions [38]. We use a weighted matrix to compensate for these differences. The outputs of all ON and OFF detectors are combined to obtain a response $R(\omega, \lambda, t)$ which encodes the temporal frequency:

$$R(\omega, \lambda, t) = \frac{1}{2} \int_{t-\xi}^{t} \iint w(x, y) \times [D^+(x, y, t) + D^-(x, y, t)] dx dy dt \tag{10}$$

where $w(x, y)$ is a weight matrix simulating the honeybee's perspective, which is defined below:

$$w(x, y) = \frac{1}{\cos \theta_{x,y} + 1}. \tag{11}$$

where $\theta_{x,y} \in (0, \pi/2)$ represents the view angle of the pixel biased from center.

However, it is hard to derive angular velocity directly from (10). Therefore, we take one detector initially in order to analyze how the response is affected by the input signals. If S_A, and S_B respectively denote the luminance changes of ommatidium A (left) and B (right), and S_A^D, S_B^D respectively denote the temporal delayed luminance changes of A and B, then according to the structure of HR-balanced detector, the response of the detector R_0 can be expressed as $\overline{S_A^D \cdot S_B - \alpha S_B^D \cdot S_A}$, where the overline means that the response is averaged over a period T to remove fluctuations caused by an oscillatory input. For simplicity, we assume the image contrast is constant during this period. Thus the response of one detector R_0 to a moving sinusoidal grating can be roughly expressed [20] using the following equation:

$$R_0 \approx \frac{C^2}{2(1+C)^2} [\sin(\frac{2\pi(\varphi + \tau\omega)}{\lambda}) - \alpha \sin(\frac{2\pi(\varphi - \tau\omega)}{\lambda})]. \tag{12}$$

By analyzing how the response R_0 changes as ω varies when presented with gratings of different spatial periods, we decode the angular velocity information from the response $R(\omega, \lambda, t)$ using an approximation method. Though there is an inevitable fitting error, we can decrease it into an acceptable level if the fitting function is chosen well. One decoding function can be chosen to approximate the actual angular velocity:

$$\widehat{\omega}(t) = a\widehat{\lambda}^{b}(t)(1 + 1/\widehat{C}(t))\sqrt{R(\omega, \lambda, t)} \tag{13}$$

where $\widehat{\omega}$ denotes the decoded angular velocity, $\widehat{C}(t)$ is the averaged estimated spatial period, and $\widehat{\lambda}(t)$ is the image contrast over a short time, derived from the texture estimation layer, a is scale parameter and b is used to tune the spatial independence. Here, $a(1 + 1/\widehat{C})\sqrt{R}$ can be seen as an estimation of the temporal frequency and has a little fitting error. The decoding function can then be explained as the ratio of the temporal frequency to the spatial frequency, which represents angular velocity. Note that $\widehat{C}(t)$ is not zero. When $\widehat{C}(t)$ approaches zero, R goes to zero, thereby preventing the decoded angular velocity reaching infinity.

4. Constant angular velocity flight control

4.1. Control Scheme for Tunnel Centering

By utilizing the physics engine of the Unity development platform, the AVDM has been embodied in a virtual honeybee to simulate the bee's tunnel centering behavior. A honeybee can center itself in a narrow tunnel by balancing the angular velocities perceived by both eyes [1]. Following this visual flight strategy, an AVDM-based control scheme is required to reproduce this behavior. The performance of the model can then be investigated by checking whether the virtual bee can center itself in a tunnel in the same way as a real bee.

The control scheme for tunnel centering is described in Fig. 3. For simplicity, the forward flight speed is held constant, and we have focused on centering using only the horizontal position controller, exploiting the difference between the angular velocities estimated by the AVDM on both eyes. Only the lateral rather than the frontal visual field is utilized in our simulation. We also assume that the orientation of the head is roughly parallel to the central path of the tunnel and is seldom affected by body movement. Interestingly, honeybees actually achieve this by performing gaze stabilizations in flight by using head yaw in advance of body yaw to cancel out rotation [39].

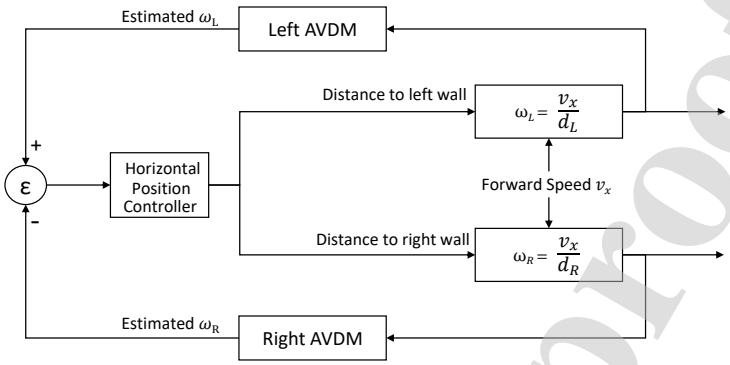

Figure 3: The AVDM-based closed loop control scheme for tunnel centering. The horizontal position controller is triggered by the difference ε between angular velocities estimated by left and right eyes.

Following the scheme, the virtual bee can adjust its position in a tunnel automatically using visual information only, in real time. The distance to the left wall will increase if the difference ε is positive and vice versa. With little modification, the scheme can be additionally used to simulate situations when one of the walls is moving along or against the flight direction. The control algorithm is also given in Algorithm 1 to summarize the tunnel centering procedure of the proposed scheme.

4.2. Control Scheme for Automatic Terrain Following

Honeybees will adjust their flight altitudes to restore a preferred ventral angular velocity if a grating moves along the flight direction. This angular velocity regulating strategy helps honeybees navigate safely through tunnels [4]. This visual strategy is also used in aircraft automatic terrain following experiments [23]. The proposed model can be inspected in this flight task to see if it can improve the accuracy of angular velocity regulation. Using the AVDM, we can estimate the angular velocity in flight. By regulating it to a constant value, the altitude will change automatically regardless of the prior knowledge of the exact altitude and forward flight speed.

The closed loop control scheme for terrain following is given in Fig 4. For

Algorithm 1: Tunnel centering algorithm

Input: initial distance to left wall d_0, initial distance to entrance x_0, integer history size $m = 10$, iteration index $i = 1$, max iteration number n;

Output: the trajectory of the virtual bee

$$T = ((d_0, x_0), (d_1, x_1), ..., (d_n, x_n))$$

while $i < m$ **do**
  Receive Image from left $I_L(i)$ and Image from right $I_R(i)$;
  Update $d_{i+1} = d_i$, $x_{i+1} = x_i + \Delta x$;
end
while $m \leq i < n$ **do**
  Receive Image $I_L(i)$ and calculate angular velocity $\omega_L(i)$ using AVDM;
  Receive Image $I_R(i)$ and calculate angular velocity $\omega_R(i)$ using AVDM;
  Update $d_{i+1} = d_i + \Delta d * Sign(\omega_L(i) - \omega_R(i))$, $x_{i+1} = x_i + \Delta x$, i = i+1;
  Discard image frame $I_L(i-m), I_R(i-m)$ from memory storage;
end
Return the trajectory T;

simplicity, we assume the forward flight speed is maintained by a constant forward thrust. This assumption is reasonable, since honeybees tend to adjust their flight height rather than speed to regulate the ventral angular velocity [4]. Thereby, the proposed AVDM can adjust the vertical lift according to the difference between the preset angular velocity and the consecutive estimated values [40]. Here, the preset angular velocity is also estimated by the AVDM in the initial phase when the vertical lift is set to the same value of gravity and where the ground is flat. Subsequently, when the ventral angular velocity varies because of terrain undulations, the vertical lift controller will change the

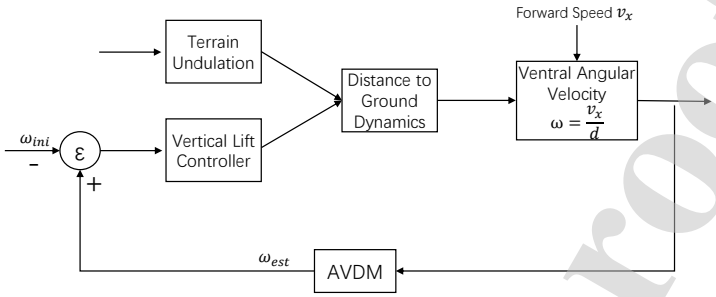

Figure 4: The AVDM-based closed loop control scheme for terrain following. The vertical lift controller is triggered by the difference ε between preset angular velocity ω_{ini} and the estimated angular velocity ω_{est}.

lift according to the difference ε between estimated ventral angular velocity and the preset value. If the difference ε is positive, the lift will increase and vice versa.

During terrain following, the vertical speed v_z is relatively small, and the air resistance can be approximated as $f = kv_z$. The vertical dynamics can then be described using the following differential equations:

$$m\frac{dv_z}{dt} = F - kv_z - mg \tag{14}$$

$$F = \rho(\omega_{est} - \omega_{ini}) \tag{15}$$

$$v_z = \frac{dz}{dt} \tag{16}$$

where m is the mass of the virtual bee, g is the gravity acceleration and F is the vertical lift, ρ is a gain control parameter. Given the initial conditions, the flight trajectory can be computed step by step. This process can be achieved in real time using the physics engine of the Unity development platform.

4.3. Parameter Setting

Parameters of the proposed model and the control scheme are shown in **Table 1**. Parameters are mainly tuned manually based on empirical knowledge and remain constant in the following simulations unless stated otherwise.

Algorithm 2: Terrain following algorithm

Input: initial height to ground h_0, initial horizontal position x_0, integer history size $m = 10$, iteration index $i = 1$, max iteration number n; preset angular velocity

Output: the trajectory of the virtual bee

$$T = ((h_0, x_0), (h_1, x_1), ..., (h_n, x_n))$$

while $i < m$ **do**
    Receive Image from ventral camera $I_V(i)$;
    Update $h_{i+1} = h_i$, $x_{i+1} = x_i + \Delta x$;
end
while $m \leq i < n$ **do**
    Receive Image $I_V(i)$ and calculate angular velocity $\omega(i)$ using AVDM;
    Adjust the vertical lift according to (14); Calculate the vertical position change Δh according to (15) and (16);
    Update $h_{i+1} = h_i + \Delta h$, $x_{i+1} = x_i + \Delta x$, i = i+1;
    Discard image frame $I_V(i - m)$ from memory storage;
end
Return the trajectory T;

5. Results

Within this section, we present the experiments and results. To demonstrate its spatial independence and robustness to contrast and noise, the proposed model is initially tested in Matlab (© The MathWorks, Inc.)using synthetic grating stimuli. The model is then implemented in the form of an agent within the Unity real-time development platform (© Unity Technologies) to reproduce the tunnel centering and terrain following behaviors of honeybees in virtual environments. Unity software permits a virtual environment to be modelled, and for algorithms to be readily attached to objects.

Table 1: Parameters of the model and the control schemes

Eq.	Parameters
(4)	$\varphi = 2^\circ,\ M = 60, N = 66$
(6)	$\sigma = 1.5$
(8)	$\mu = 1$
(9)	$\tau = 0.005\ s,\ \alpha = 0.25$
(10)	$\xi = 0.05s$
(13)	$a = 100\ \mathrm{s}^{-1},\ b = 1$
(14)	$k = 0.1\ \mathrm{kg/s},\ g = 9.81\ \mathrm{m/s}^2$
(15)	$\rho = 0.04\ \mathrm{kg \cdot m/s}$
(17)	$p = 1$

5.1. Angular velocity decoding results

To inspect the spatial frequency independence of the proposed model, sinusoidal gratings of a wide range of spatial periods (12° to 72°) are chosen as the visual inputs. The results of estimated angular velocities are shown in Fig. 5. The proposed model decodes the angular velocity well with little variance, except when dealing with a narrow grating (12°) that moves at a high angular velocity (larger than $700^\circ/s$). Honeybees tend to maintain a constant angular velocity of $300^\circ/s$ [41], around which our proposed AVDM fits well and represents large spatial independence. Here we use adjusted R-squared, a statistical indicator that quantifies how well the data points fit the ground truth line, to evaluate the decoding errors. The adjusted R-squared values for different spatial periods are provide in **Table 2**. As can be seen, most of the decoding curves estimate the angular velocity well since the adjusted R-squared values are close to 1. This means the AVDM performs in a stable manner and estimates the angular velocity against a wide range of spatial periods, explaining how honeybees navigate well in a cluttered environment.

In order to demonstrate the improved spatial independence of the AVDM compared with the state-of-the-art angular velocity estimation models, we con-

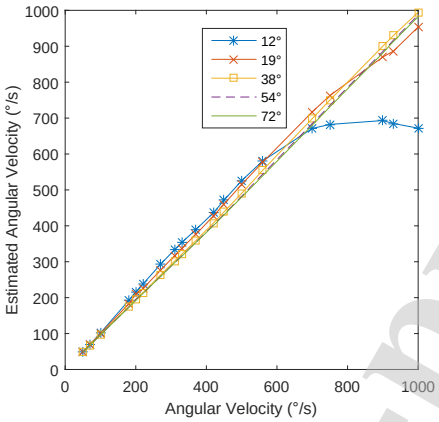

Figure 5: The angular velocity decoding results. The estimated angular velocity curves under different angular velocities when tested by moving gratings of different spatial periods (12°, 19°, 38°, 54° and 72°), demonstrating the spatial frequency independence of the model.

Table 2: The adjusted R-squared values of angular velocity decoding curves of different spatial periods.

Spatial Period	12°	19°	38°	54°	72°
Adjusted-R^2	0.8685	0.9962	0.9995	0.9981	0.9974

trast it with two other aforementioned detection models, the R-HR model [11] and the C-HR model [12]. The original results of these models are re-plotted in Fig. 6 under the same metric. The AVDM responses have also been rectified into (0, 1) by a Lipetz transformation [15]. The Lipetz transformation is specified by the following equation to introduce a saturating nonlinearity:

$$U = R^p/(R^p + R_0), \tag{17}$$

where R is the input response, p is an exponent in (0.5, 1], R_0 is a parameter defining a middle response level.

Here, we introduce a new indicator, Averaged Spatial Independence Deviation, which uses the standard deviation of the normalized responses when tested by moving gratings of different spatial periods. A comparison of spatial independence from the three models is shown in Fig. 7. With the indicator, the spatial

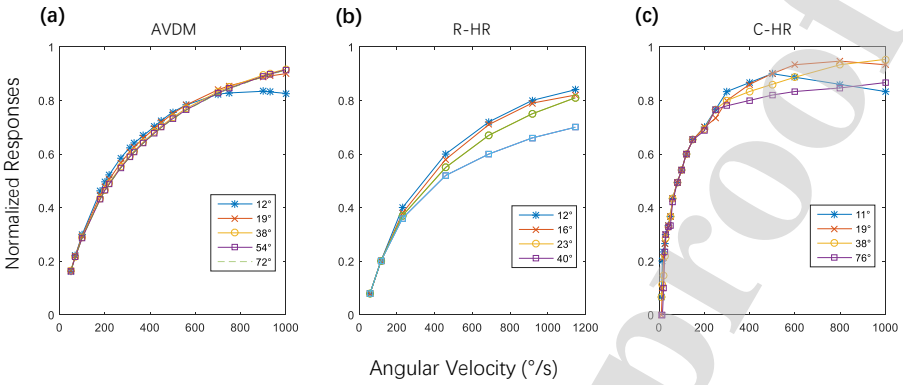

Figure 6: **Comparison of normalized responses with two other published models.** (a) The normalized responses of AVDM by a Lipetz transformation. (b) Response curves of the R-HR model for different spatial periods at various angular velocities [11]. (c) The normalized responses of C-HR model shows a large spatial independence around the velocity of 100 $^\circ/s$ [12].

independence of the model responses can now be evaluated at any angular velocity. In general, our model shows a stronger spatial independence than the other models. The R-HR model shows a larger response variation when angular velocity increases. The C-HR model performs well at around $100^\circ/s$, but shows a larger deviation at low (less than $60^\circ/s$) and high (faster than $300^\circ/s$) angular velocities. Compared with the comparative models, our proposed AVDM performs better to decode angular velocities in a larger range.

Honeybees can navigate proficiently in a tunnel with a range of contrasting wall patterns [32]. To evaluate the robustness of the model towards image contrast, we test the proposed model by moving sinusoidal gratings of different contrasts. As can be seen from Fig. 8(a), the results show little variance when the image contrast varies from 1/5 to 3/5. This outperforms previous models, especially when the angular velocity is low or high [12]. The proposed model processes the texture estimation pathway where the contrast is first estimated, and the decoding layer where the estimated contrast is used, to decode the angular velocity. The angular velocity is estimated accurately despite the contrast

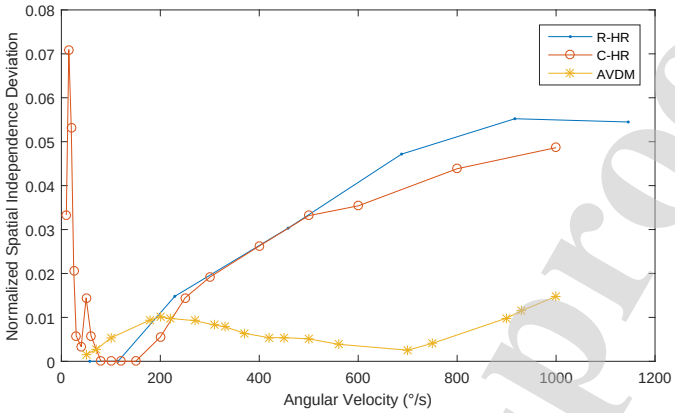

Figure 7: Comparing spatial independence with two other models. The Averaged Spatial Independence Deviation for three models have been given to show their performance at various angular velocities. The proposed AVDM shows lower deviations in a large range of angular velocities.

dynamics of input stimuli, reminiscent of honeybee's flights through dynamic and cluttered environments.

To demonstrate the robustness of the proposed model to noise, we perform a test in which we incorporate differing levels of Gaussian white noise into the input signals. The results are shown in Fig. 8(b). The estimated image velocity curves show little variance when the signal-to-noise ratio (SNR) is larger than 40 dB. The results demonstrate the reliability of the AVDM when being implemented into small robots since normal cameras usually have a SNR of 50 dB or higher.

5.2. Tunnel centering simulation results

In real tunnel behavioral experiments, honeybees can fly along the center of the patterned tunnel even when the walls are covered with gratings of different spatial frequencies or contrasts[1]. Biologists suggest that honeybees can estimate the background speed independent of the spatial frequency and contrast, and adjust their positions by balancing the angular velocity sensed by their two compound eyes. Therefore, reproducing similar flight behaviors is one of the

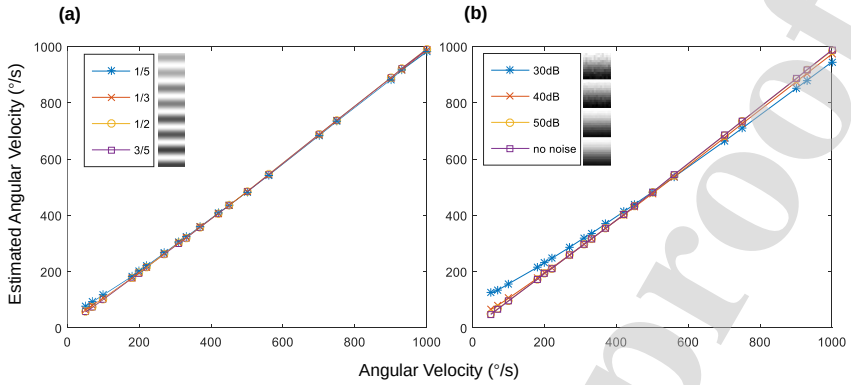

Figure 8: Robustness of the proposed AVDM against contrast and noise. (a) The proposed model is tested by the moving sinusoidal gratings of 54° spatial period and the image contrasts are set as 1/5, 1/3, 1/2 and 3/5. (b) The proposed model is tested by the moving sinusoidal gratings of 54° spatial period and the SNR of the input gratings are set as 30 dB, 40 dB and 50 dB. The result of the input without noise is also given as a reference.

criteria we can evaluate to check the model performance in this situation. Lots of corridor experiments on centering and speed regulation have been performed to demonstrate the navigation ability of their bioinspired wide field optic flow integration model [42, 43].

To verify the effectiveness of the proposed model, we aim to reproduce tunnel centering behaviors of honeybees as closely as possible. The virtual environment is set up, again using the Unity platform (see Fig. 9). A series of simulations have been performed, including centering from different lateral positions, a large independence towards spatial frequency of the gratings, X-shape tunnel centering and lateral position adjustment with a moving wall.

In the first kind of simulations, the virtual bee starts at different positions in the patterned tunnel. We implement the AVDM in both eyes of the virtual bee, and then assess if the bee can perform a centering response in the same way as a real bee. In one of the simulations, both walls are covered with patterns of the same spatial frequency (46 cycles m^{-1}) as shown in Fig. 10. Although the virtual bee is released at different start points, it can adjust its position using only visual information and will eventually fly along the central path of

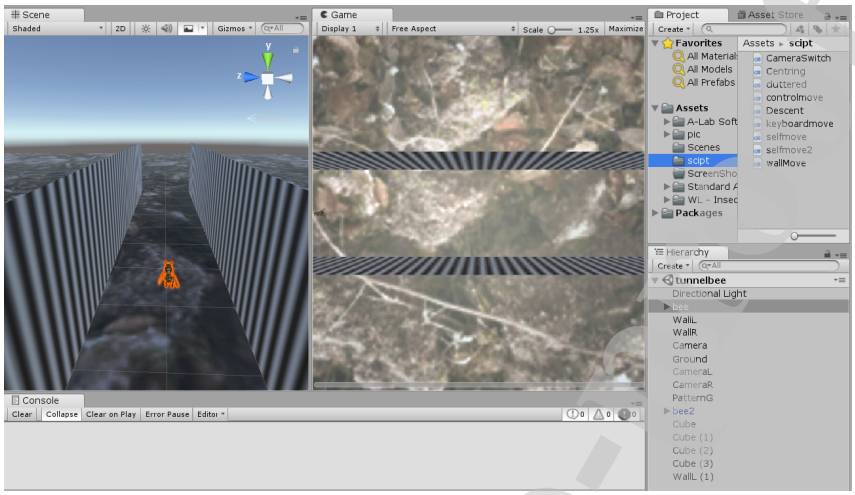

Figure 9: Unity simulation environment of the tunnel experiments. The virtual bee flies in a simulated tunnel with sinusoidal patterns on both walls. The images received by two eyes can be processed separately in real time to regulate the route of the flight. A demo video can be found at `https://youtu.be/gNvtaSqNjdI`.

the tunnel. The results remain unaltered if the spatial frequencies are changed (15, 20, 30, 40 cycles m^{-1}) so long as the two walls carry the same pattern.

In the second kind of simulations, the spatial independence of the proposed model is investigated by changing the spatial frequency of one wall while keeping it constant in the other wall. As can be seen in Fig. 11, though the spatial frequency of the right wall varies considerably, the virtual bee still manages to fly along the tunnel with little bias from the central path. This is in accordance with the results of biological experiments which showed that the centering response is barely affected by the spatial frequency of the pattern [44]. The bias may be caused by the difference between the estimated angular velocities when tested with different patterns (see Fig. 6). This means the model is not fully spatially independent. However, behavioral experiments with real bumblebees reveal that similar phenomenon can be observed in this situation [45]. This indicates that a large, rather than full spatial independence might be implemented in the neural system of the real bee.

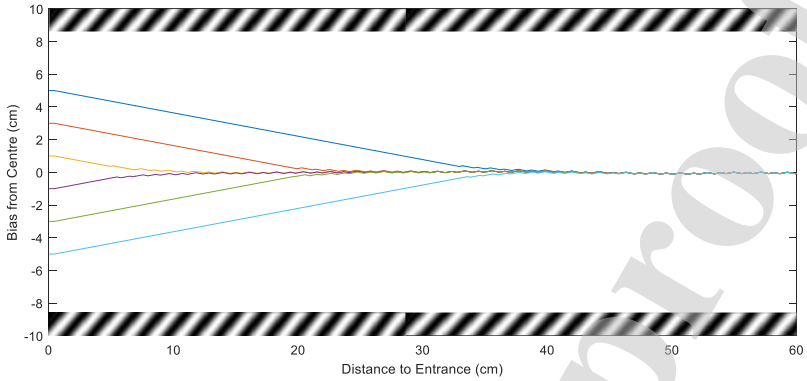

Figure 10: Tunnel centering from different start points. Routes of the virtual bee with AVDM implemented are recorded when they fly through the patterned tunnel from different start points. The flight paths are adjusted by the control scheme in Fig. 4.

In the third series of simulations, the virtual bee is further evaluated using an X-shape tunnel of which the width first decreases and then increases. Real bees can not only perform centering, but also reduce speed as the tunnel gets narrower to restore a preferred image velocity [44, 46] in this situation. In order to reproduce the speed adjustment behavior in an X-shape tunnel, a feedback control scheme is designed within our simulation to regulate the sum of angular velocities estimated by both eyes to a constant value. The results are shown in Fig. 12. Though released at different start points, the bee adjusts its lateral position to fly towards the central path. In addition, the flight speed is altered as the width varies, further indicating the practicality of the proposed model.

All three kinds of tunnel simulations reproduce similar behaviors of real bees in a patterned tunnel. However, this is not enough to show that the proposed model is able to effectively estimate the angular velocity. For example, a model capable of gauging distance to the walls using visual information can produce similar centering responses too. In tunnel experiments honeybees will shift towards one wall if the wall moves along the same direction of their flights, and shift towards the opposite side if the wall moves in the opposite direction to balance the angular velocities on both sides [47]. This lateral position adjustment

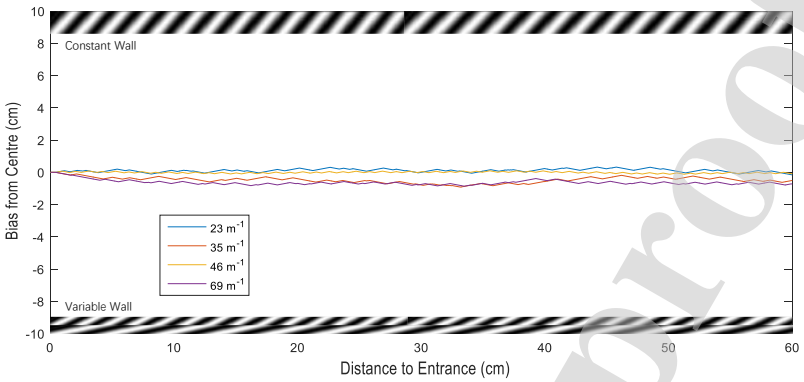

Figure 11: Tunnel centering with gratings of different spatial frequencies. The left wall is always carrying gratings of spatial frequency of 46 cycles m^{-1} while the spatial frequency of right wall grating varies from 23, 35, 46, 69 cycles m^{-1}. The trajectories show the robustness of the centering towards spatial frequency.

indicates that honeybees do adjust positions by balancing the angular velocities rather than the distances to walls.

In order to demonstrate that the proposed model works well in this scenario, simulations with moving walls have been designed. The results are shown in Fig. 13. The virtual bee moves closer to the left wall if the left wall is moving along the flight direction at a constant speed (much slower than the flight speed). The lateral position shifts as expected to balance the angular velocities estimated on both eyes. In contrast, the trajectory of the virtual bee shifts to the right wall if the left wall is moving backward. Both coincide with the results of behavioral experiments on honeybee visual control [47], indicating that the proposed model can explain the tunnel centering behaviors of honeybees effectively.

5.3. Terrain following simulation results

The accuracy of the model in estimating angular velocity has not been fully demonstrated by the tunnel centering experiments. This is because the control scheme is triggered by the difference between the angular velocities estimated by each of the two eyes. The error in the estimation of angular velocity may be decreased by subtraction. To further verify the effectiveness of the proposed

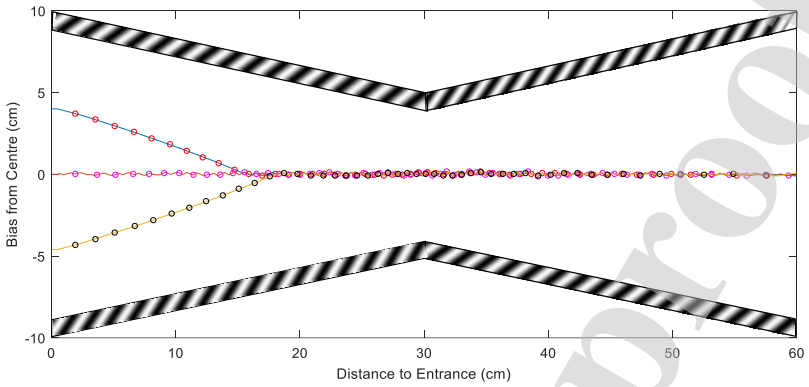

Figure 12: X-shape Tunnel centering simulations. The flight trajectories of the virtual bee, starting from different points, are shown in the same graph. The walls of the tunnel are covered with sinusoidal gratings of spatial frequency of 46 cycles m^{-1}. The positions of the agent are marked by circles separated by a same time.

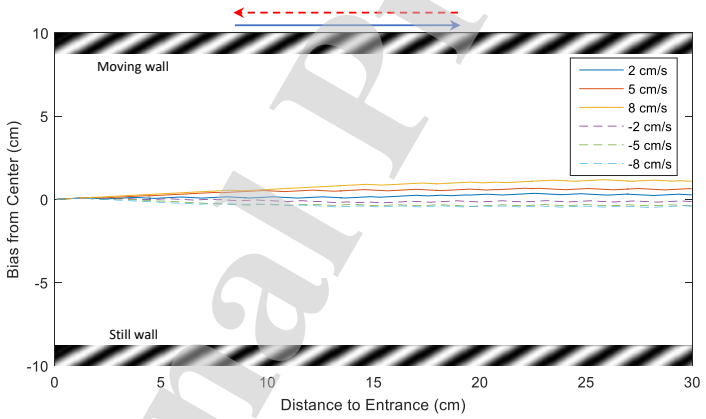

Figure 13: Tunnel centering when one wall moving forward or backward at various speeds. The solid line indicates that one wall is moving forward, and the dot line represents that the wall is moving backward. The agent flight speed is 30 cm/s.

model, the AVDM is implemented in a virtual bee in terrain following simulations where the ground is covered with gratings (see Fig. 14). The performance of this visually guided flight task depends more on the accuracy of angular velocity estimation, providing an ideal opportunity to examine our proposed model. A series of terrain following simulations have been designed. The flight

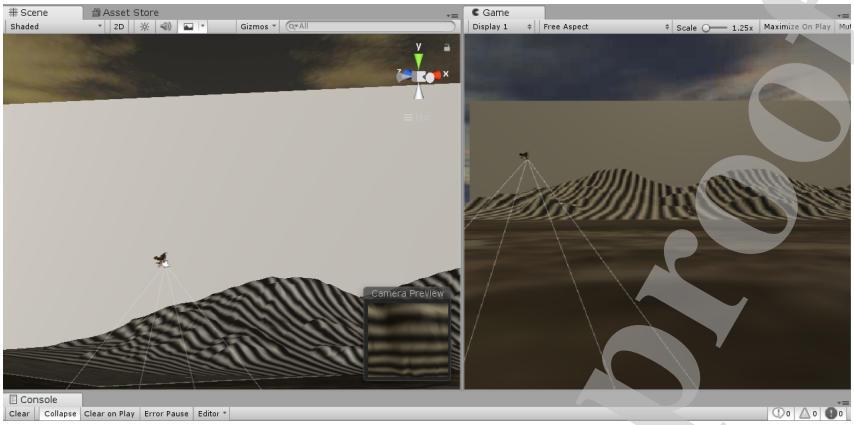

Figure 14: Unity simulation environment of the terrain following experiments. The bee flies over an undulating terrain with nonuniform sinusoidal grating using only ventral visual information. A demonstration video is given at `https://youtu.be/l3SAnmOrgfk`.

trajectories and the ventral responses have been recorded to see if the virtual bee can perform automatic terrain following using only visual information by estimating the angular velocity of image motion and regulating it to a constant value.

The virtual bee with the AVDM is first tested on a regular terrain covered with sinusoidal gratings. The virtual bee is released at around a given height (25 cm) with a certain forward speed (50 cm/s). Initially, the bee is set to fly forward without changing its altitude (by setting the vertical lift equal to its gravity). The preset angular velocity value is then estimated using the AVDM after the first few frames. By regulating the consecutive angular velocities to this preset value using the control scheme described in the previous section (Fig. 5), the aim is that the flight altitude will be adjusted automatically using only visual information. The result is shown in Fig. 15.

As can be seen, the angular velocity estimated by the ventral camera is accurate and remains constant when the bee flies over flat terrain, except for during the first few frames. The ventral response increases when the bee flies closer to the undulating terrain, and vice versa. By changing the vertical lift

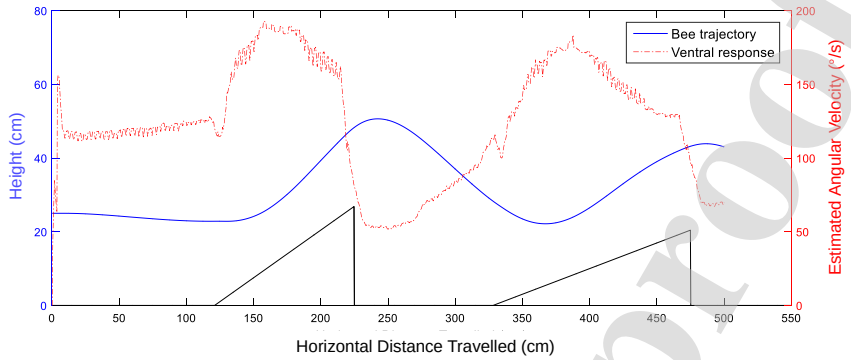

Figure 15: Terrain following flight trajectory and estimated angular velocities. The bee flight trajectory is recorded when flying over a terrain (black line) with sinusoidal gratings (30 cycles m^{-1}), and the angular velocities that are estimated by the ventral eye are also shown indicating how the trajectory is affected by angular velocity regulation.

according to the difference between estimated angular velocities and the preset value, the virtual bee always maintains a suitable distance from textured ground. Information on the flight speed or the flight altitude is unnecessary to perform this visually guided task. In general, the proposed AVDM works sufficiently to navigate the bee whilst flying over the patterned regular terrain. Similar terrain following experiments have been performed using aircraft [21, 23]. The main difference is that they use the EMD sensor's output rather than angular velocity to regulate the flight course. Our proposed model directly estimates the angular velocity to improve the accuracy of the regulation in terrain following.

To inspect the robustness of terrain following under various conditions, a series of controlled trials have been performed. First, the virtual bee is released at different initial heights. The terrain following trajectories are shown in Fig. 16(a). As can be seen, the virtual bee follows the terrain well by maintaining distances according to the initial heights above the ground. The presetting of the angular velocity ensures the bee follows the terrain proficiently with dynamic initial heights. The lower the initial height is, the better the flight trajectory follows the terrain. When the initial height is 50 cm, the ventral angular velocity varies less since the undulation of the terrain is relatively smaller at this height

than at lower heights.

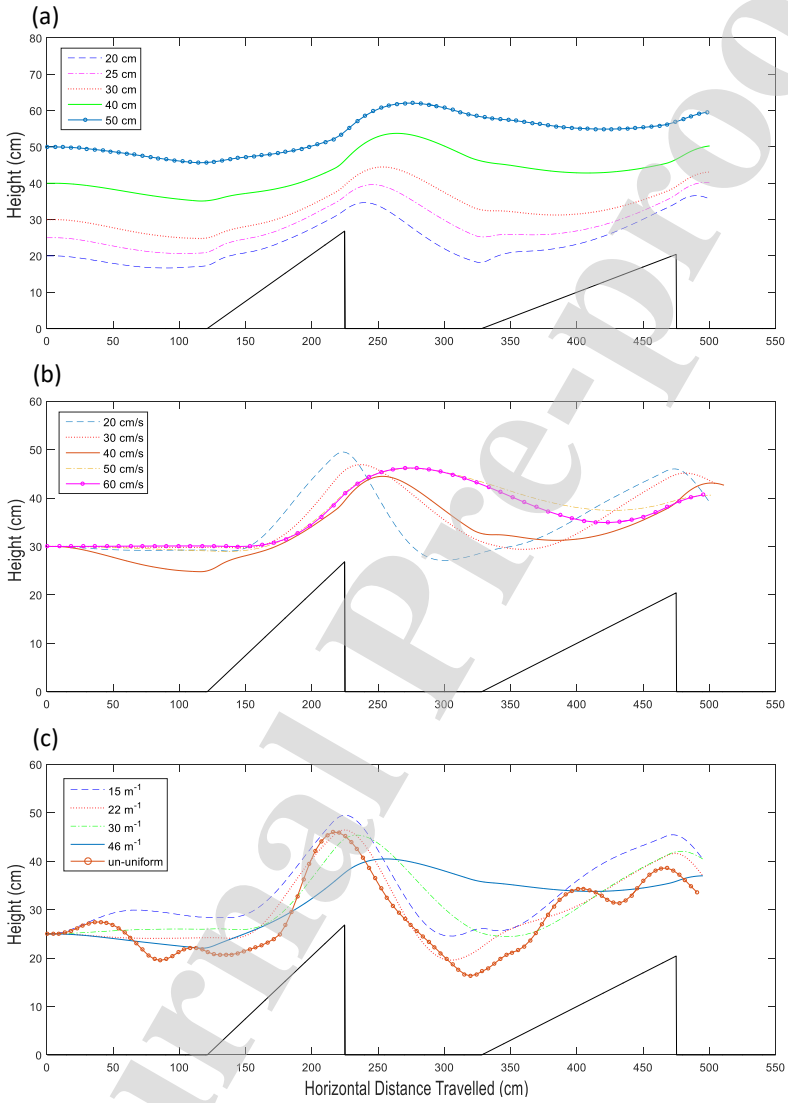

Figure 16: Controlled trials showing the robustness of terrain following at different flight heights, speeds and terrain gratings. (a) The virtual bee is released at different initial heights with a speed of 50 cm/s to fly over the terrain with a sinusoidal grating (30 cycles m^{-1}). (b) The virtual bee is released with different flight speeds at a height of 30 cm to fly over the terrain with a sinusoidal grating (30 cycles m^{-1}). (c) The virtual bee is released with a flight speed of 40 cm/s at a height of 25 cm to fly over the terrain with different gratings.

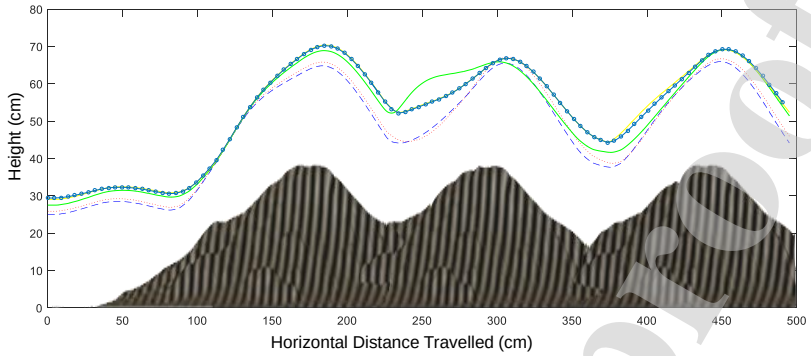

Figure 17: Multiple flight trajectories of terrain following over the mountain shaped terrain with sinusoidal gratings. The trajectories fit the undulation of the patterned mountain well with slightly different initial heights and speeds which shows the robustness of the model and control scheme.

In the second kind of controlled trials, the influence of the flight speed on terrain following is investigated. The flight speed is chosen from 20 cm/s to 60 cm/s, and the trajectories are recorded in Fig. 16(b). The trajectories of all tested speeds follow the terrain well using only visual information without any danger of crashing. The differences among trajectories are mainly caused by the control scheme. The trajectory follows the terrain very well if the speed is 20 cm/s. It is harder to adjust the flight height smoothly if the virtual bee flies faster. A better control scheme may improve the performance of terrain following at different speeds.

Finally, the spatial independence of the proposed model in terrain following is evaluated by covering the terrain with different gratings (see Fig. 16(c)). A wide range within spatial periods of gratings are chosen. All flight trajectories follow the terrain well given the same initial flight height and flight speed. It is clear from the flight trajectories over gratings with different spatial frequencies (Fig. 16(c)), that spatial frequency has a small effect on terrain following performance. Again, it fulfills our expectation of large rather than full spatial independence of the proposed model.

To see whether the model is stable under more complex scenarios, we also

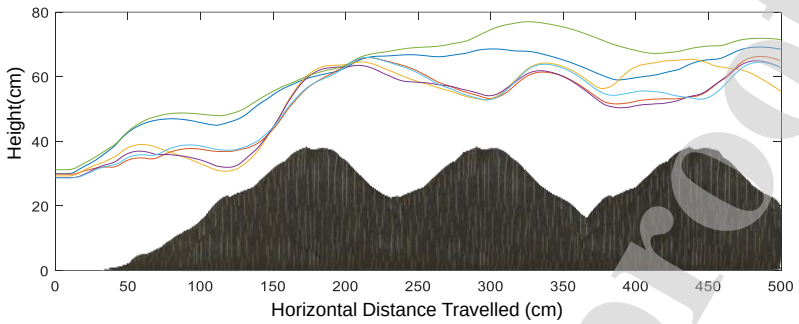

Figure 18: Multiple flight trajectories of terrain following over carpet texture. The successful terrain following over a mountain covered with natural carpet texture shows the potential for application in flight control of MAVs.

tested the virtual bee above a mountain shaped terrain with irregular undulations and covered with sinusoidal gratings. The result is shown in Fig. 17. The flight trajectories show that the flight altitude changes automatically according to the distance from the ground by regulating the angular velocity. Whenever the bee gets closer to the ground, the increasing angular velocity estimated by the AVDM will trigger the controller to provide a higher vertical lift to help the bee rise away from the ground. The robustness of the model and control scheme have been further verified using a carpet texture (see Fig. 18). Though the terrain following of the mountain undulations in this situation is not as good as the terrain following over sinusoidal gratings, the bee still flies over the terrain successfully at slightly different heights and speeds. This further verifies the effectiveness of the proposed AVDM in the terrain following simulations, showing the potential of applying in MAV's flight control.

6. Discussion and Conclusion

We have presented an angular velocity decoding model (AVDM), which estimates the speed of visual motion by combining both textural and temporal information from input signals. The model comprises three parts: elementary motion detection circuits, a wide-field texture estimation pathway and an an-

gular velocity decoding layer. When initially tested with moving sinusoidal gratings, the model estimates angular velocity highly effectively with improved spatial frequency independence when compared with the state-of-the-art angular velocity detection models. The model has been further evaluated for the ability to reproduce tunnel centering and terrain following behaviors. We have considered the spatial and temporal resolutions of honeybees to obtain bio-plausible parameter settings for explaining these behaviors. A previous model [48] by Cope et al. fits the electrophysiological data [9] better. However, we have not tried to fit data with large variances. We have focused on reducing the spatial dependence with the aim of simulating the visual flight behaviors more effectively. We consider that there is a trade-off between biological plausibility and algorithmic efficiency. Our approximation of the nonlinear relationship might not be the way bees decode the angular velocity, but it functions sufficiently to reproduce their visual flights behaviors.

Although the proposed model is designed primarily for estimating angular velocity using sinusoidal gratings, it can be easily generalized to deal with other patterns. In fact, even without any modification, the AVDM works well enough to decode angular velocity against patterns with clear edges such as a checkerboard pattern with a range of spatial frequencies. The model has been further tested against an irregular snow mountain terrain[14] and a carpet textured terrain. The flight trajectory does not follow the terrain as well as it does when the mountain terrain is covered with sinusoidal gratings. However, trajectories of successful flights whilst avoiding crashing indicate the considerable potential of the model to navigate well in cluttered environments.

There are several potential impacts of our work. Most directly, our work may be used to research other visually guided flight behaviors such as visual landing. Our code and demonstration videos are publicly available. The simulations can be established easily on the same platform, though motion dynamics and control schemes might be different for specific visual flight tasks. Moreover, the model can also be employed in MAVs for visual flight using visual sensors alone. Compared with traditional methods, the computational effort of our proposed

method has been reduced significantly in two ways. Firstly, the image size required to decode the angular velocity is small and secondly, the computation is reduced by use of discrete integrals. It should be noted that, neuromorphic sensing is often used in many insect-like robots to reduce computation [49, 50].

In addition, the proposed model has the potential to simulate other behaviors of honeybees. For example, maintaining a constant angular velocity is also used in honeybee wall following behavior [3, 51]. Integrating the angular velocity can also provide odometric information. This may help to explain how honeybees gauge flight distance[6]. As for the model itself, we provide motion detectors only for the progressive and regressive directions. Motion detectors for upward and downward movement could also be incorporated to form a more complete visual detection system for dealing with more complex and dynamic visual scenes.

Acknowledgment

This research is supported in part by the EU HORIZON 2020 projects, STEP2DYNA under grant 691154 and ULTRACEPT under grant 778062; and in part by the National Natural Science Foundation of China under grant 12031003 and 11771347; and in part by the China Postdoctoral Science Foundation under grant 2020M682651. The authors would like to thank the handling editor and the anonymous reviewers for their careful reading and helpful remarks, which have contributed towards improving the quality of this paper.

References

[1] M. Srinivasan, S. Zhang, M. Lehrer, T. Collett, Honeybee navigation en route to the goal: visual flight control and odometry, Journal of Experimental Biology 199 (1) (1996) 237–244.

[2] E. Baird, M. V. Srinivasan, S. Zhang, R. Lamont, A. Cowling, Visual control of flight speed and height in the honeybee, in: International Conference on Simulation of Adaptive Behavior, Springer, 2006, pp. 40–51.

[3] J. R. Serres, G. P. Masson, F. Ruffier, N. Franceschini, A bee in the corridor: centering and wall-following, Naturwissenschaften 95 (12) (2008) 1181.

[4] G. Portelli, F. Ruffier, N. Franceschini, Honeybees change their height to restore their optic flow, Journal of Comparative Physiology A 196 (4) (2010) 307–313.

[5] J. R. Serres, F. Ruffier, Optic flow-based collision-free strategies: From insects to robots, Arthropod structure & development 46 (5) (2017) 703–717.

[6] H. Esch, J. Burns, Honeybees use optic flow to measure the distance of a food source, Naturwissenschaften 82 (1) (1995) 38–40.

[7] M. V. Srinivasan, M. Poteser, K. Kral, Motion detection in insect orientation and navigation, Vision research 39 (16) (1999) 2749–2766.

[8] M. V. Srinivasan, S. W. Zhang, J. S. Chahl, E. Barth, S. Venkatesh, How honeybees make grazing landings on flat surfaces, Biological cybernetics 83 (3) (2000) 171–183.

[9] M. Ibbotson, Evidence for velocity–tuned motion-sensitive descending neurons in the honeybee, Proceedings of the Royal Society of London B: Biological Sciences 268 (1482) (2001) 2195–2201.

[10] M. Ibbotson, Y. Hung, H. Meffin, N. Boeddeker, M. Srinivasan, Neural basis of forward flight control and landing in honeybees, Scientific reports 7 (1) (2017) 14591.

[11] O. Riabinina, A. O. Philippides, A model of visual detection of angular speed for bees, Journal of theoretical biology 257 (1) (2009) 61–72.

[12] A. J. Cope, C. Sabo, K. Gurney, E. Vasilaki, J. A. Marshall, A model for an angular velocity-tuned motion detector accounting for deviations in the corridor-centering response of the bee, PLoS computational biology 12 (5) (2016) e1004887.

[13] H. Wang, Q. Fu, H. Wang, J. Peng, P. Baxter, C. Hu, S. Yue, Angular velocity estimation of image motion mimicking the honeybee tunnel centring behaviour, in: The 2019 International Joint Conference on Neural Networks, IEEE, 2019.

[14] H. Wang, Q. Fu, H. Wang, J. Peng, S. Yue, Constant angular velocity regulation for visually guided terrain following, in: IFIP International Conference on Artificial Intelligence Applications and Innovations, Springer, 2019, pp. 597–608.

[15] P. A. Shoemaker, D. C. O'carroll, A. D. Straw, Velocity constancy and models for wide-field visual motion detection in insects, Biological cybernetics 93 (4) (2005) 275–287.

[16] D. J. Fleet, Measurement of image velocity, Vol. 169, Springer Science & Business Media, 2012.

[17] P. Zhu, J. Isaacs, B. Fu, S. Ferrari, Deep learning feature extraction for target recognition and classification in underwater sonar images, in: 2017 IEEE 56th Annual Conference on Decision and Control (CDC), IEEE, 2017, pp. 2724–2731.

[18] A. Borst, T. Euler, Seeing things in motion: models, circuits, and mechanisms, Neuron 71 (6) (2011) 974–994.

[19] B. Hassenstein, W. Reichardt, Systemtheoretische analyse der zeit-, reihenfolgen-und vorzeichenauswertung bei der bewegungsperzeption des rüsselkäfers chlorophanus, Zeitschrift für Naturforschung B 11 (9-10) (1956) 513–524.

[20] J. M. Zanker, M. V. Srinivasan, M. Egelhaaf, Speed tuning in elementary motion detectors of the correlation type, Biological cybernetics 80 (2) (1999) 109–116.

[21] F. Ruffier, N. Franceschini, Optic flow regulation: the key to aircraft automatic guidance, Robotics and Autonomous Systems 50 (4) (2005) 177–194.

[22] N. Franceschini, F. Ruffier, J. Serres, A bio-inspired flying robot sheds light on insect piloting abilities, Current Biology 17 (4) (2007) 329–335.

[23] F. Ruffier, N. Franceschini, Optic flow regulation in unsteady environments: A tethered mav achieves terrain following and targeted landing over a moving platform, Journal of Intelligent & Robotic Systems 79 (2) (2015) 275–293.

[24] H. Wang, J. Peng, P. Baxter, C. Zhang, Z. Wang, S. Yue, A model for detection of angular velocity of image motion based on the temporal tuning of the drosophila, in: International Conference on Artificial Neural Networks, Springer, 2018, pp. 37–46.

[25] M. Egelhaaf, R. Kern, J. P. Lindemann, Motion as a source of environmental information: a fresh view on biological motion computation by insect brains, Frontiers in neural circuits 8 (2014) 127.

[26] J. Li, J. Lindemann, M. Egelhaaf, Local motion adaptation enhances the representation of spatial structure at emd arrays, PLoS computational biology 13 (12) (2017) e1005919.

[27] R. A. Seidl, Die sehfelder und ommatidien divergenzwinkel von arbeiterin, königin und drohn der honigbiene (apis mellifica), Ph.D. thesis (1982).

[28] S. Laughlin, G. Horridge, Angular sensitivity of the retinula cells of dark-adapted worker bee, Zeitschrift für vergleichende Physiologie 74 (3) (1971) 329–335.

[29] H. Autrum, M. Stoecker, Die verschmelzungsfrequenzen des bienenauges, Zeitschrift für Naturforschung B 5 (1) (1950) 38–43.

[30] M. V. Srinivasan, M. Lehrer, Temporal acuity of honeybee vision: behavioural studies using moving stimuli, Journal of Comparative Physiology A 155 (3) (1984) 297–312.

[31] M. Roper, C. Fernando, L. Chittka, Insect bio-inspired neural network provides new evidence on how simple feature detectors can enable complex visual generalization and stimulus location invariance in the miniature brain of honeybees, PLoS computational biology 13 (2) (2017) e1005333.

[32] A. Chakravarthi, S. Rajus, A. Kelber, M. Dacke, E. Baird, Differences in spatial resolution and contrast sensitivity of flight control in the honeybees apis cerana and apis mellifera, Journal of Experimental Biology 221 (20) (2018) jeb184267.

[33] Q. Fu, H. Wang, C. Hu, S. Yue, Towards computational models and applications of insect visual systems for motion perception: A review, Artificial life 25 (3) (2019) 263–311.

[34] S. Yue, F. C. Rind, Collision detection in complex dynamic scenes using an lgmd-based visual neural network with feature enhancement, IEEE Trans. Neural Netw. 17 (3) (2006) 705–716.

[35] Q. Fu, C. Hu, J. Peng, S. Yue, Shaping the collision selectivity in a looming sensitive neuron model with parallel on and off pathways and spike frequency adaptation, Neural Networks 106 (2018) 127–143.

[36] F. Pinto-Teixeira, C. Koo, A. M. Rossi, N. Neriec, C. Bertet, X. Li, A. Del-Valle-Rodriguez, C. Desplan, Development of concurrent retinotopic maps in the fly motion detection circuit, Cell 173 (2) (2018) 485–498.

[37] W. Stürzl, N. Böddeker, L. Dittmar, M. Egelhaaf, Mimicking honeybee eyes with a 280 field of view catadioptric imaging system, Bioinspiration & biomimetics 5 (3) (2010) 036002.

[38] Q. Fu, H. Wang, J. Peng, S. Yue, Improved collision perception neuronal system model with adaptive inhibition mechanism and evolutionary learning, IEEE Access 8 (2020) 108896–108912.

[39] N. Boeddeker, L. Dittmar, W. Stürzl, M. Egelhaaf, The fine structure of honeybee head and body yaw movements in a homing task, Proceedings

of the Royal Society of London B: Biological Sciences 277 (1689) (2010) 1899–1906.

[40] J. Gemerek, S. Ferrari, B. H. Wang, M. E. Campbell, Video-guided camera control for target tracking and following, IFAC-PapersOnLine 51 (34) (2019) 176–183.

[41] E. Baird, M. V. Srinivasan, S. Zhang, A. Cowling, Visual control of flight speed in honeybees, Journal of experimental biology 208 (20) (2005) 3895–3905.

[42] J. S. Humbert, A. M. Hyslop, Bioinspired visuomotor convergence, IEEE Transactions on Robotics 26 (1) (2009) 121–130.

[43] T. S. Clawson, T. C. Stewart, C. Eliasmith, S. Ferrari, An adaptive spiking neural controller for flapping insect-scale robots, in: 2017 IEEE Symposium Series on Computational Intelligence (SSCI), IEEE, 2017, pp. 1–7.

[44] M. V. Srinivasan, Honey bees as a model for vision, perception, and cognition, Annual review of entomology 55 (2010) 267–284.

[45] J. P. Dyhr, C. M. Higgins, The spatial frequency tuning of optic-flow-dependent behaviors in the bumblebee bombus impatiens, Journal of Experimental Biology 213 (10) (2010) 1643–1650.

[46] M. V. Srinivasan, Visual control of navigation in insects and its relevance for robotics, Current opinion in neurobiology 21 (4) (2011) 535–543.

[47] M. Srinivasan, S. Zhang, Visual control of honeybee flight, in: Orientation and communication in arthropods, Springer, 1997, pp. 95–113.

[48] A. J. Cope, C. Sabo, E. Vasilaki, A. B. Barron, J. A. Marshall, A computational model of the integration of landmarks and motion in the insect central complex, PloS one 12 (2) (2017) e0172325.

[49] A. Vanarse, A. Osseiran, A. Rassau, A review of current neuromorphic approaches for vision, auditory, and olfactory sensors, Frontiers in neuroscience 10 (2016) 115.

[50] G. Indiveri, S.-C. Liu, Memory and information processing in neuromorphic systems, Proceedings of the IEEE 103 (8) (2015) 1379–1397.

[51] F. L. Roubieu, J. R. Serres, F. Colonnier, N. Franceschini, S. Viollet, F. Ruffier, A biomimetic vision-based hovercraft accounts for bees' complex behaviour in various corridors, Bioinspiration & biomimetics 9 (3) (2014) 036003.

Declaration of interests

☒ The authors declare that they have no known competing financial interests or personal relationships that could have appeared to influence the work reported in this paper.

☐The authors declare the following financial interests/personal relationships which may be considered as potential competing interests: